Preprint
UCRL-JC-139843

Backscatter reduction using combined spatial, temporal, and polarization beam smoothing in a long scalelength laser-plasma

J.D. Moody, B.J. MacGowan, J.E. Rothenberg, R.L. Berger, L. Divol, S.H. Glenzer, R.K. Kirkwood, E.A. Williams and P.E. Young

This article was submitted to Physical Review Letters

U.S. Department of Energy
Lawrence Livermore National Laboratory

June 27, 2000

Backscatter reduction using combined spatial, temporal, and polarization beam smoothing in a long scalelength laser-plasma

J. D. Moody, B. J. MacGowan, J. E. Rothenberg, R. L. Berger, L. Divol[1], S. H. Glenzer, R. K. Kirkwood, E. A. Williams, and P. E. Young

Lawrence Livermore National Laboratory

University of California

Livermore, CA 94551

and

[1]*CEA/DIF BP 12 91680 Bruyères-Le-Châtel, France*

Abstract

Spatial, temporal, and polarization smoothing schemes are combined for the first time to reduce to a few percent the total stimulated backscatter of a NIF-like probe laser beam (2×10^{15} W/cm^2, 351-nm, f/8) in a long scalelength laser plasma. Combining temporal and polarization smoothing reduces SBS and SRS up to an order of magnitude although neither smoothing scheme by itself is uniformly effective. The SRS spectra are more monochromatic with more beam smoothing, a trend consistent with reduction of filamentation. The results agree with trends observed in F3D simulations [R. L. Berger et al., Phys. Plasma **6**, 1043 (1999)].

PACS numbers: 52.38.-r, 52.35.-g, 52.35.Mw, 52.50.Jm

The present schemes for inertial-confinement-fusion (ICF) target ignition require a highly symmetric illumination of the fuel capsule by x-rays (indirect drive) or laser light (direct drive)[1]. The current point design for the National Ignition Facility (NIF) indirect drive hohlraum target [2] consists of a cylindrical gas filled high-Z chamber with thin polyimide windows covering both ends and a fuel pellet suspended in the center. Laser beams burn through the windows and gas to illuminate the inner wall of the hohlraum where the laser energy is converted to soft x-rays which compress the fuel capsule to high density and temperature. The low-density gas-fill effectively slows the rate at which plasma blow-off from the wall fills the hohlraum. However, both the low-density long scalelength plasma resulting from the gas-fill and the high-Z hohlraum inner wall plasma provide environments that support detrimental laser-plasma scattering instabilities.

The large-aperture glass laser systems used in ICF applications typically produce beams with irregular intensity in the form of hot-spots at focus due to inherent or heat-induced aberrations in the amplifier glass. As a result of their high intensity, these hot spots can experience substantial power losses from stimulated Brillouin scattering (SBS) and stimulated Raman scattering (SRS) [3] in a target plasma. To reduce these scattering losses, various beam-smoothing techniques have been developed to create more regular speckle intensity distributions [4,5,6,7,8,9,10,11,12]. Three particular smoothing techniques are kinoform/random phase plate (KPP/RPP) spatial smoothing[12], smoothing by spectral dispersion (SSD)[6], and polarization smoothing (PS)[7,8,9,10,11]. SSD effectively smoothes only after a speckle decorrelation time whereas the effects of PS are instantaneous. Therefore, we expect these two smoothing schemes to affect the rapidly growing SRS and slower growing SBS in different ways. Experiments investigating these techniques have been ongoing for over 10 years and have shown varying degrees of laser scattering reduction for different plasma geometries and incident laser characteristics[13]. It is important, however, to understand the effect of these smoothing techniques in NIF

plasma conditions with long density scalelengths (~ 1 mm) and high electron temperature (> 2 keV) where growth of stimulated instabilities is likely to be high and saturation mechanisms may be different than in inhomogeneous and colder plasmas.

In this Letter, we present experimental results which show that using SSD and polarization smoothing schemes in combination produces a significantly greater reduction in the total backscattering from a long scalelength gasbag plasma than expected from the reduction of backscatter seen with SSD and PS individually. In the experiments reported here, we directly compare SSD and PS with the same plasma conditions and laser parameters and, thereby, provide a true comparison of their relative efficacy. We show experimentally that, on plasma scales and with laser intensities relevant for NIF, polarization smoothing or SSD alone do not in all cases of interest effectively control LPI. However, when SSD and PS are combined, we find that SRS, SBS, and filamentation are all significantly reduced. In addition, the separate effects of SSD and PS on the instantaneous scattering give evidence for competition between the instabilities [14,15,16] in which the SBS, when large, suppresses the SRS. These results are consistent with simulations performed with the laser plasma interaction code (F3D) [17].

The experiments were conducted at the Lawrence Livermore National Laboratory using the Nova laser which provided 10 beams of λ_0=351 nm wavelength light. The target, laser, and backscatter measurement configuration was the same as what has been used in previous experiments [18]. The experiments used a gas-filled balloon [19] designed to emulate the long scalelength gas region in a NIF hohlraum. The targets were filled with various mixtures of C_5H_{12} (neopentane) and C_3H_8 (propane) gases whose ionized electron density was varied between 7.5% and 15% of the critical density for 351nm laser light. Experiments studying beam smoothing effects in targets that emulate the wall region of a NIF hohlraum have been reported earlier [20]. Nine of the Nova beams were used to heat the gasbag target and the tenth beam drove the backscatter instabilities.

Each heater beam delivers 2.2 kJ in a 1 ns square pulse, is f/4.3, does not use a phase plate, and is defocused by 6.7 mm to illuminate a large section of the gasbag surface at an intensity of about 1-2×10^{14} W/cm^2. The probe beam, with energy between 1.5 and 2.3 kJ, had a 1 ns square pulse shape, was delayed 0.4 ns relative to the heater beams, and was configured as an f/8.5 beam for these experiments. Laser light from the probe always passed through a kinoform phase plate (KPP). This KPP produced a focal spot in the shape of an ellipse measuring about 400 μm by 260 μm. The intensity envelope of the focal spot was fairly flat and dropped off rapidly near the edges. The vacuum transverse speckle size at focus is f λ_0 ~ 3 μm and the longitudinal depth of focus is $8f^2 \lambda_0$ ~ 200 μm, where f =8.5 is the F# of the probe beam focusing geometry. The backscattered light was collected over a large 25° cone angle which included light directed back into the focus lens as well as light scattered outside of the lens.

Application of SSD in these experiments leads to a laser phase[6] at the final focusing lens given by $\phi(t,y) = \omega_0 t + \alpha \sin\left(\omega_{fm} t + \beta y\right)$ where $\omega_0 = 2\pi c / \lambda_0$, c is the speed of light, t is time, βy is related to the phase shift across the lens due to the SSD grating dispersion and $\nu_{fm} = \omega_{fm} / 2\pi$ =17 GHz is the modulation frequency. The SSD grating produces a ~ 150 ps delay or ~ 2 color cycles across the circular aperture. The focal spot consists of the time-dependent interference of speckle patterns from the frequencies within the laser bandwidth, $\Delta\nu = 2\alpha\nu_{fm}$. The interference pattern decorrelates in about 5 ps (for $\alpha = 7$), which is sufficiently fast to reduce SBS[21] and filamentation growth, but does not significantly affect the much faster SRS[17].

The polarization smoothing implemented in the Nova experiments used a 2x2 array of birefringent wedges [8] (27 cm square KDP crystals cut at an angle of 41.2° to the optic axis), similar to the beam arrangement planned for NIF. The wedges divided the incident 351 nm light into two equal-power, orthogonally-polarized beams having a slight angular

separation, $\Delta\theta$, from each other. This scheme is depicted in Fig. 1. After passing through the KPP, the two orthogonally polarized beams form identical speckle patterns in the focal plane shifted by the amount, $\Delta\theta \cdot F$, where the focal length, F, is 5.6 m. We chose a shift of 30 μm or about 10 speckle half-widths, larger than the minimum shift of the half-speckle width required to decorrelate a speckle pattern generated by a square near-field [11]. The direction of the PS shift was set to be approximately orthogonal to the SSD dispersion direction. Simulations of LPI don't show any significant advantage to making PS and SSD orthogonal [11] although considerations of speckle decorrelation times do [7].

Gasbag plasmas have been extensively characterized with both experimental measurement and hydrodynamic simulation[22,23]. Gated x-ray pinhole camera measurements show that the gasbag becomes heated uniformly after 0.3 to 0.4 ns. The heater beams burn to the target center in about 0.3 ns and create a fairly uniform temperature and density plasma by 0.4 ns with about a 1.5 to 2 mm scalelength. The rapid blowdown of the gasbag polyimide shell when the heater beams initially turn on launches a weak shock which propagates toward the center of the target leaving a rarefaction wave behind. Thomson scattering measurements show that the macroscopic plasma flow is small (about 4×10^6 cm/s) in the central region of the target but steadily increases outside the rarefaction wave. Helium-α, Lyman-α, and isoelectronic ratios obtained from x-ray measurements are used to determine the temporal evolution of the electron temperature[24]. These measurements show that the central temperature gradually rises during the time that the heater beams are on to a peak of about 2.6 keV for 7% n_c and 3 keV for 11% n_c where n_c is the critical density at 351 nm. Once the heaters turn off the electron temperature decreases as the plasma expands and ion and electron temperatures equilibrate.

The plasma electron density fell approximately into one of three density groups, 8%, 10%, and 15% of critical density for 351 nm. As the density increased over this range the backscattered light fraction increased for SRS and decreased for SBS. At low density the SBS tended to dominate the overall scattering whereas at high density the SRS dominated [16].

Direct comparison of smoothing techniques in identical plasma conditions is shown in Figs. 2 (a)-(d). The data shows that the combination of SSD and the KPP reduces SBS [Fig. 2(a)] without significantly changing the amount of SRS [Fig. 2(b)] while, addition of PS to the KPP causes both the SBS and SRS to decrease at all densities [Figs. 2(c) and (d)]. To quantitatively compare the effects of the smoothing techniques we define f_{PS}, f_{SSD}, and f_{PS+SSD} as the ratio of the total backscattered fraction (SBS + SRS) for each of the three combinations (PS+KPP, SSD+KPP, and PS+SSD+KPP, respectively) to the total backscattered fraction using the KPP alone. So, f_{PS} = 0.7 at ~0.08n_c and f_{PS} = 0.57 at ~0.10n_c. In comparison, f_{SSD} = 0.8 for ~0.08n_c and 0.9 for ~0.10n_c. Uncertainty in the backscatter measurement is estimated to be about 20%.

The effects of PS and SSD are enhanced by using them in combination. Application of both 250 GHz of SSD[25] and PS leads to the lowest level of SBS and SRS at each density as shown by the solid diamond symbols in Figs. 2 (c) and (d). In this case, f_{PS+SSD} = 0.3 at ~0.08n_c density and 0.23 at ~0.10n_c. We see that $f_{PS+SSD} < f_{PS} \cdot f_{SSD}$ where the reduction factor, $f_{PS+SSD} / f_{PS} \cdot f_{SSD}$, is about 0.5 for the ~0.08n_c and ~0.10n_c cases[26]. Similar results are observed at the higher density ~0.15n_c where the reduction is about 0.7. F3D simulations for similar conditions (0.10n_c, T_e = 3 keV, I = 2x10^{15} W/cm^2 and axial length equal to 1/3 of the gasbag density plateau length)[17] but less total gain than calculated for these experiments predict a reduction factor of 0.1 resulting from the combination of SSD and PS. To the extent that the gasbag plasma is representative of the

plasma in the central section of a NIF hohlraum, these results show that NIF may benefit from polarization smoothing of the inner beams which pass through the longest region of plasma before reaching the hohlraum wall.

Competition between SRS and SBS [14,15,16] is suggested in the SSD data where Figs. 2 (a) and (b) compare the scattering fraction with KPP and KPP + 250 GHz of SSD. Adding SSD reduces the SBS but leads to either an increase or no change in the SRS. Figure 3 shows a comparison of the time histories for SRS and SBS with KPP only and KPP + 375 GHz SSD. We show a case with 50% larger bandwidth to display more clearly the change in time history of the SRS signal. This time history is typical of SRS signals at 250 GHz SSD. At the time of peak electron temperature (1 ns) SSD strongly reduces the SBS but increases the SRS. Linear instability theory that neglects competition would predict that both the SBS and SRS should decrease when SSD is applied. In this case the SSD would suppress filamentation [27] and the resulting formation of high intensity speckles which tend to produce the majority of the SRS and SBS backscattered light. A consistent explanation of the data follows if, for example, the SBS (without SSD) extracts a large fraction of the power in the high intensity speckles. Then, reducing the SBS with SSD increases the laser power available to SRS. We note that there may be other competition mechanisms [28,29] that produce a similar result. Polarization smoothing, showing a marked contrast to SSD, causes both the SRS and SBS to decrease without much change in either one's pulse shape.

The efficacy of PS and SSD on laser plasma instabilities can be understood qualitatively in terms of the convective growth rates of the instabilities compared to the smoothing rate. In general, filamentation has the slowest growth rate ($\gamma_{fil} < 10^{12}$ sec^{-1}), SRS the fastest ($\gamma_{srs} \sim 10^{13}$ sec^{-1}), and SBS is intermediate between the others ($\gamma_{sbs} \sim 2 \times 10^{12}$ sec^{-1}) where the growth rate estimates pertain to the experimental parameters, $n_e = 1 \times 10^{21}$

cm^{-3}, T_e = 3 keV, T_i = 0.8 keV, and <I> = $2x10^{15}$ W/cm^2. The bandwidth, $\Delta\omega$ ($=2\pi\Delta\nu$), is 1.6 x 10^{12} sec^{-1} for 250 GHz SSD. Since the bandwidth is about the same as the SBS growth rate, the statistical theory result that $\gamma = \gamma_0^2/\Delta\omega$ does not apply[30]. However, recent theory[21] has shown that if the bandwidth changes the speckle pattern before the instability has grown to saturation, a significant reduction may occur. That is the case in this experiment. Thus, we anticipate that SSD in our experiments will not directly affect SRS, will have some effect on SBS, and will substantially reduce filamentation. Polarization smoothing on the other hand is instantaneous and is expected to reduce all instabilities and in particular SRS.

These experiments and recent F3D simulations of the effect of SSD and PS on SRS and SBS [17,31] confirm these expectations. In both the calculations and the experiments, SSD was shown to be rather ineffective in reducing SRS although it reduced SBS. Filamentation was reduced in the simulations and we infer from changes to the SRS spectra, in which it became more narrow and more red shifted[20,32], that it was also reduced in the experiments by SSD. In addition, PS was effective at reducing SRS, SBS, and filamentation in both the simulations and the experiments. Finally, the combination of SSD and PS was shown to be particularly effective, again both in the calculations and the experimental data, because PS instantaneously reduced the growth rate such that the bandwidth became comparable to the convective growth rate in a substantial fraction of the hotspots. The competition between SRS and SBS plays a role in the effect of beam smoothing on any one of the instabilities because, for example, as less power is extracted from a hotspot by one instability, the growth rate for the other is reduced less.

In conclusion, our polarization smoothing experiments suggest that this technique, because of its instantaneous effect, can significantly improve the margin against plasma instabilities when combined with smoothing by spectral dispersion. This is still the case

even at the higher intensities and densities expected in 350-eV ignition target designs. One could thereby increase the operating region available to the NIF for ICF experiments. The effects of PS and SSD on the SRS and SBS are in qualitative agreement with 3D simulations of SRS and SBS.

Acknowledgements

The authors acknowledge the contributions of C. Geddes, L. Suter, E. Lefebvre, A. B. Langdon, and C. H. Still. This work was performed under the auspices of the U. S. Department of Energy by the Lawrence Livermore National Laboratory under Contract No. W-7405-ENG-48.

Figure Captions:

Figure 1. Schematic showing the use of a birefringent wedge to generate two shifted and orthogonally polarized speckle patterns for beam smoothing.

Figure 2. Experimental measurements of (a) the stimulated Brillouin and (b) the stimulated Raman scattered light in gasbag plasmas for KPP only and KPP + 250 GHz SSD [$\Delta\lambda / \lambda_0 = 3$Å/1054Å]. Comparison of the three different smoothing combinations KPP, KPP + PS, and KPP + SSD + PS show different effects on (c) SBS and (d) SRS backscattering. The probe intensity is 2×10^{15} W/cm^2, except at the high density, where it is 5×10^{15} W/cm^2. All measurements are made at the time of peak electron temperature (1 ns).

Figure 3. Time history of the SRS and SBS scattered light from a 10% critical plasma shows a higher instantaneous SRS backscatter level for KPP + 375 GHz SSD than for KPP only whereas the SBS shows a large reduction with SSD.

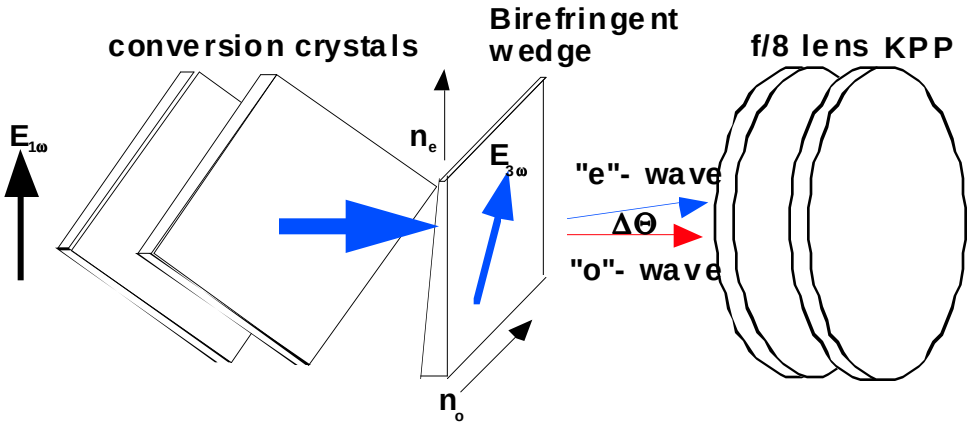

Figure 1. Schematic showing the use of a birefringent wedge to generate two shifted and orthogonally polarized speckle patterns for beam smoothing.

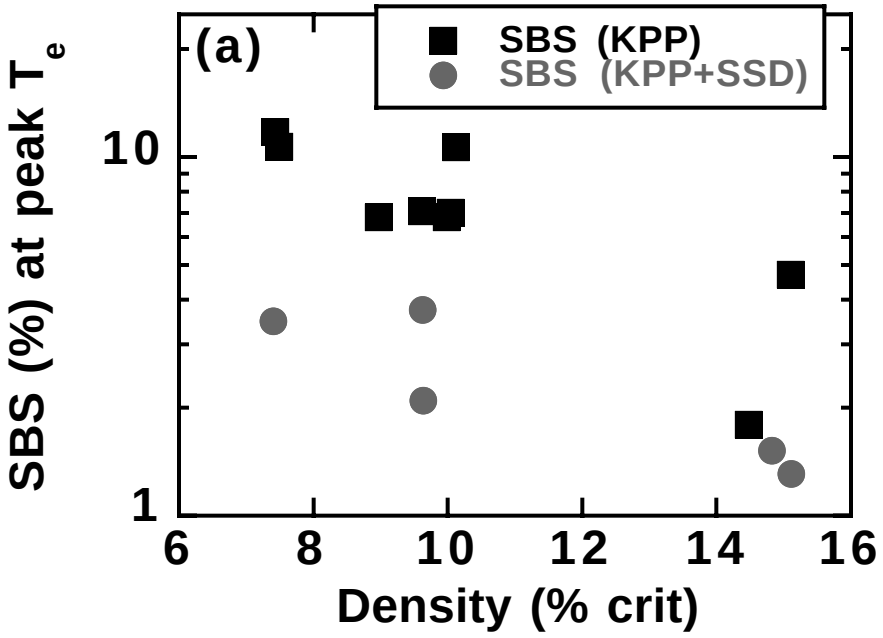
(a)
SBS (KPP)
SBS (KPP+SSD)
SBS (%) at peak T_e
10
1
6
8
10
12
14
16
Density (% crit)

Figure 2 (a).

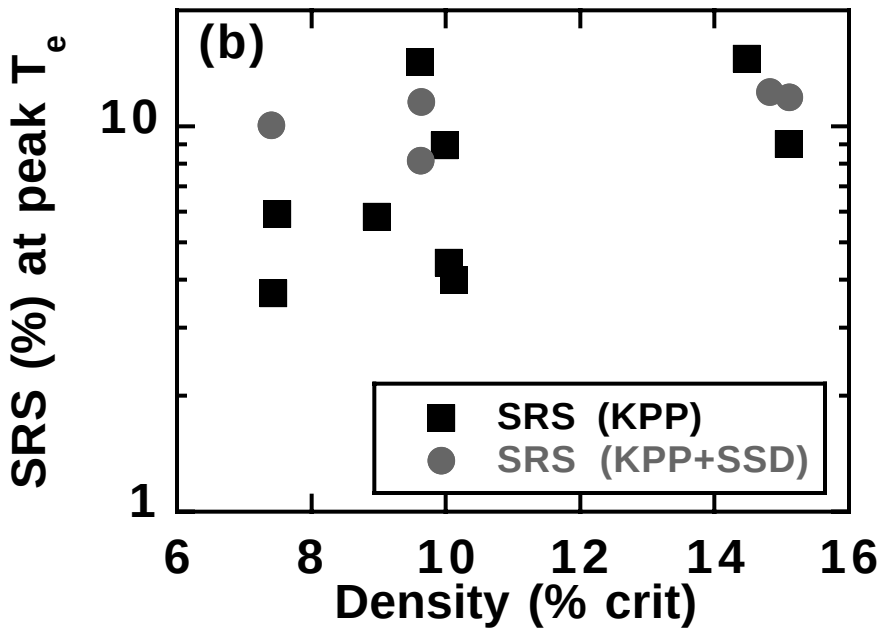
(b)
SRS (%) at peak T_e
10
1
6
8
10
12
14
16
Density (% crit)
SRS (KPP)
SRS (KPP+SSD)

Figure 2 (b).

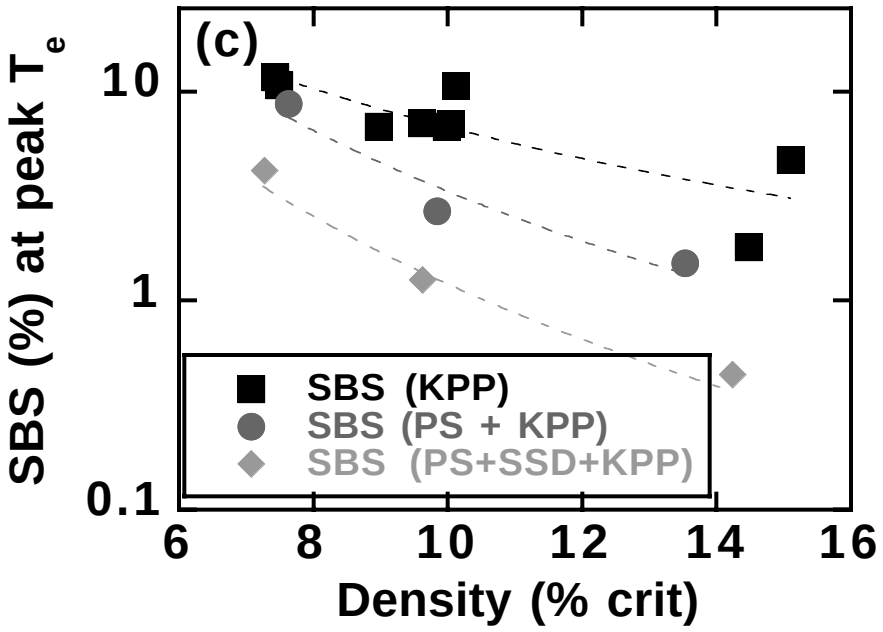
(c)
SBS (%) at peak T_e
10
1
0.1
6
8
10
12
14
16
Density (% crit)
SBS (KPP)
SBS (PS + KPP)
SBS (PS+SSD+KPP)

Figure 2 (c).

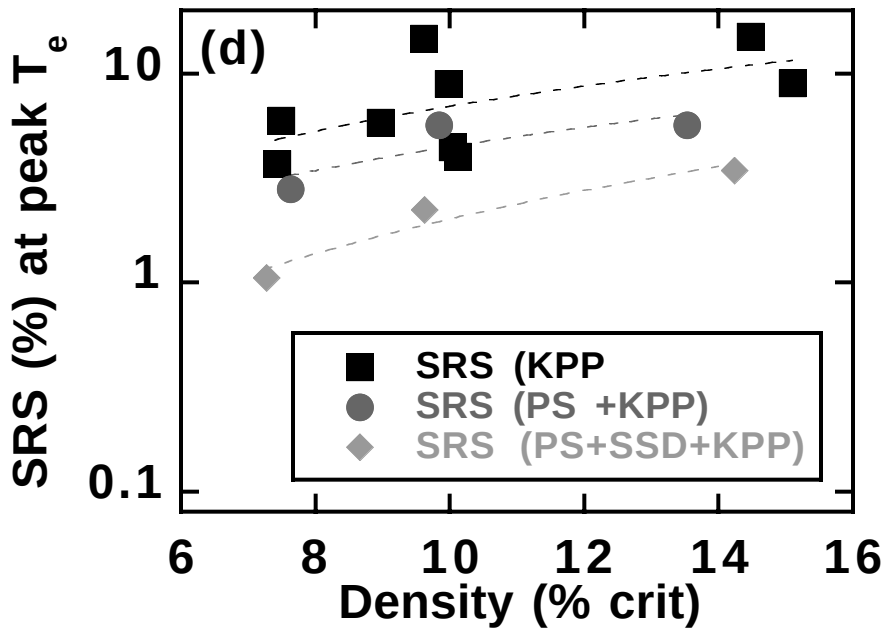

Figure 2 (d).

Figure 2 caption: Experimental measurements of (a) the stimulated Brillouin and (b) the stimulated Raman scattered light in gasbag plasmas for KPP only and KPP + 250 GHz SSD [$\Delta\lambda/\lambda_0$ =3Å/1054Å]. Comparison of the three different smoothing combinations KPP, KPP + PS, and KPP + SSD + PS show different effects on (c) SBS and (d) SRS backscattering. The probe intensity is $2x10^{15}$ W/cm^2, except at the high density, where it is $5x10^{15}$ W/cm^2. All measurements are made at the time of peak electron temperature (1 ns).

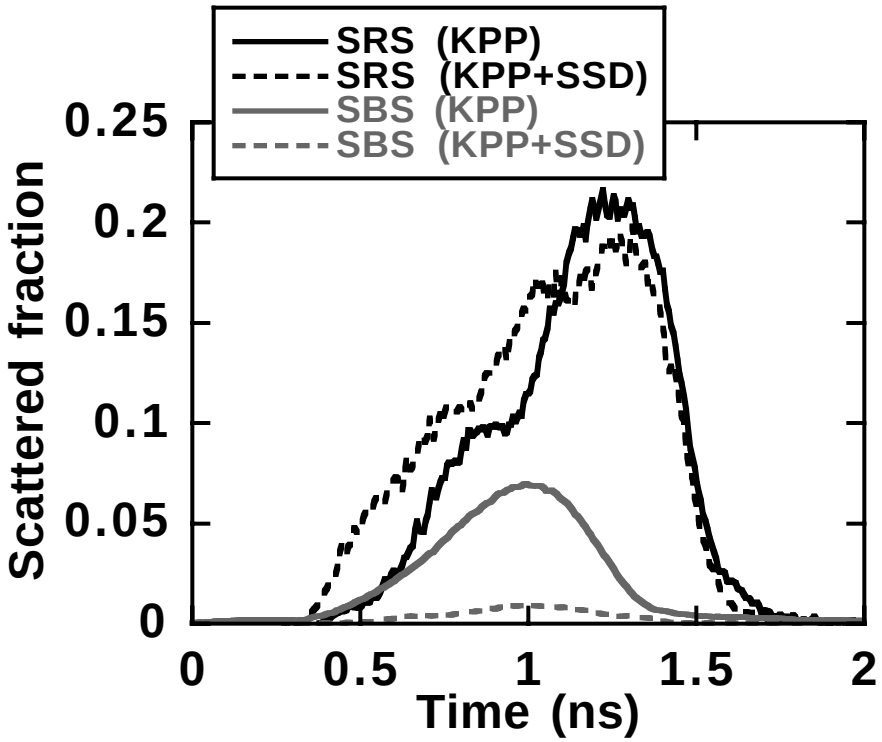

Figure 3. Time history of the SRS and SBS scattered light from a 10% critical plasma shows a higher instantaneous SRS backscatter level for KPP + 375 GHz SSD than for KPP only whereas the SBS shows a large reduction with SSD.

References

1. J. D. Lindl, *Phys. Plasmas* **2**, 3933 (1995).

2. S. W. Haan, et al. , *Phys. Plasmas* **2**, 2480 (1995).

3. R. L. Kauffman, et al., *Phys. Rev. Lett.* **73**, 2320 (1994).

4. R. H. Lehmberg and S. P. Obenschain, *Optics Comm.* **46**, 27 (1983); R. H. Lehmberg and J. Goldhar, *Fusion Technology* **11**, 532-541 (1987).

5. Y. Kato, et al., *Phys. Rev. Lett.* **53**, 1057-1060 (1984).

6. S. Skupsky, R. W. Short, T. Kessler, R. S. Craxton, S. Letzring, and J. M. Soures, *J. Appl. Phys.* **66**, 3456 (1989).

7. J. E. Rothenberg, Proc. Soc. Photo-Opt. Instrum. Eng. **2633**, 634 (1995). J. E. Rothenberg, *Journal of Applied Physics* **87**, 3654 (2000).

8. "Phase Conversion Using Distributed Polarization Rotation," LLE review **45**, 1-12 (1990).

9. K. Tsubakimoto, et al., *Opt. Commun.* **91**, 9-12 (1992); K. Tsubakimoto, et al., *Opt. Commun.* **103**, 185-188 (1993).

10. S. Pau, S. N. Dixit, and D. Eimerl, "Electro-Optic Control of Correlations in Speckle Statistics," *J. Opt. Soc. Am.* B **11**, 1498 (1994).

11. E. Lefebvre, et al., *Phys. Plasmas* **5**, 2701 (1998).

12. S. N. Dixit, et al., *Opt. Lett.* **19**, 417 (1994).

13. See, for example, O. Willi, et al., Phys. Fluids B **2**, 1318 (1990) and C. Labaune, et al., Phys. Fluids B **4**, 2224 (1992).

14. J. Fuchs, et al., *Phys. Rev. Lett.* **84**, 3089 (2000).

15. C. J. Walsh, et al., Phys. Rev. Lett. 53, 1445 (1984); D. M. Villeuneuve, et al., *Phys. Rev. Lett.* **59**, 1585 (1987); H. A. Baldis, et al., *Phys. Rev. Lett.* **62**, 2829 (1989); C. Labaune, et al., *Phys. Plasmas* **4**, 423 (1997).

16. D. S. Montgomery, et al., *Phys. Plasmas* **5**, 1973 (1998).

17. R. L. Berger, et al., *Phys. Plasmas* **6**, 1043 (1999).

18. B. J. MacGowan, et al, *Phys. Plasmas* **3**, 2029 (1996).

19. D. H. Kalantar, et al., *Phys. Plasmas* **2**, 3161 (1995).

20. S. H. Glenzer, *et al*, *Phys. Rev. Lett.* **80**, 2845 (1998).

References cont.

21. Ph. Mounaix, et al., *Phys. Rev. Lett.* **85**, 4526 (2000).

22. J. J. Denavit and D. W. Phillion, *Phys. Plasmas* **1**, 1971 (1994).

23. L. V. Powers, et al., *Phys. Plasmas* **2**, 2473 (1995).

24. S. H. Glenzer, et al., *Phys. Rev. E* **55**, 927 (1997).

25. 250 Ghz refers to the laser bandwidth in cycles/sec, ν, defined earlier.

26. If SSD and PS do not interact with each other and their effects are characterized as simply causing a reduction in the reflectivity of the plasma then their combined effect is expected to be $f_{PS} \cdot f_{SSD}$.

27. The SRS data indicates that SSD does reduce filamentation since the SRS spectrum is narrower with SSD than with KPP-only.

28. H. A. Rose, *Phys. Plasmas* **4**, 437 (1997).

29. M. Curtet and G. Bonnaud, *Phys. Rev. E.* **5**, 5052 (1999); W. Rozmus et al. *Phys. Fluids* **26**, 1071 (1983).

30. G. Laval, et al., *Phys. Fluids* **20**, 2049 (1977)

31. R. L. Berger, et al., *Phys. Plasmas* **5**, 4337 (1998).

32. Y. Kato, *et al*. *Phys. Rev. Lett*. **53**, 1057 (1984); C. Labaune *et al*. *Phys. Fluids* B**4**, 2224 (1992).